PHYSICAL REVIEW E **94**, 043101 (2016)

Multiscaling in superfluid turbulence: A shell-model study

Vishwanath Shukla[1,*] and Rahul Pandit[2,†]
[1]*Laboratoire de Physique Statistique de l'Ecole Normale Supérieure, 24 Rue Lhomond, 75231 Paris, France*
[2]*Centre for Condensed Matter Theory, Department of Physics, Indian Institute of Science, Bangalore 560012, India*

(Received 5 August 2015; published 3 October 2016)

We examine the multiscaling behavior of the normal- and superfluid-velocity structure functions in three-dimensional superfluid turbulence by using a shell model for the three-dimensional (3D) Hall-Vinen-Bekharevich-Khalatnikov (HVBK) equations. Our 3D-HVBK shell model is based on the Gledzer-Okhitani-Yamada shell model. We examine the dependence of the multiscaling exponents on the normal-fluid fraction and the mutual-friction coefficients. Our extensive study of the 3D-HVBK shell model shows that the multiscaling behavior of the velocity structure functions in superfluid turbulence is more complicated than it is in fluid turbulence.

DOI: 10.1103/PhysRevE.94.043101

I. INTRODUCTION

The study of turbulence in quantum fluids is an important, challenging problem, which has witnessed a spurt of activity because of advances in experimental techniques [1–11]. This has led, in turn, to intense theoretical and numerical investigations; however, much remains to be done to obtain a good understanding of superfluid turbulence (see the excellent reviews in Refs. [12–17]).

Superfluidity occurs in a wide variety of systems, such as ^{4}He II, ^{3}He-B, Bose-Einstein condensates (BECs) of bosonic atoms in traps, and neutron stars. No single theory covers all these systems; and there is no theory that can cover all the length and time scales that are required to describe superfluid turbulence in quantum fluids. Furthermore, turbulence in such systems is influenced by the quantum properties that are manifested at the macroscopic scale. For example, liquid helium, below the superfluid transition temperature $T_\lambda = 2.17$ K, can sustain rotational motion only through the formation of quantum vortices, around which the circulation of the velocity is quantized. The following three important phenomenological approaches have been used to investigate the properties of such turbulence: (a) The first uses the Gross-Pitaevskii equation (GPE), which provides a good hydrodynamical description with resolved quantum vortices; the GPE approach works well at low temperatures and for weakly interacting bosons [18]. (b) The second uses the vortex-filament model, in which quantized vortices are regarded as filaments in three dimensions (3D), because the vortex core size $a \simeq 10^{-10}$ m (in, e.g., helium II); thus, the filaments can be treated as classical objects in many physically relevant situations, e.g., when the mean intervortex separation $\ell_v \gg a$ or the radius of curvature of the filaments [19–21]. (c) The third approach uses the two-fluid, Hall-Vinen-Bekharevich-Khalatnikov (HVBK) model, wherein we ignore the the distinction between individual, quantized vortices and deal with an effective, coarse-grained model (this HVBK model is valid only for length scales $\ell \gg \ell_v$) [22–25].

It is important to investigate how various statistical properties of classical-fluid turbulence are modified in turbulence in quantum fluids [16,26]. In particular, it behooves us to test theoretical ideas, developed for turbulence in classical fluids, in superfluid systems and then to use them to analyze experiments on quantum turbulence. For statistically homogeneous and isotropic, 3D, classical-fluid turbulence, the phenomenological 1941 theory of Kolmogorov (K41) predicts, for the fluid energy spectrum, $E(k) \sim k^{-5/3}$, for wave numbers k in the inertial range $2\pi/L \ll k \ll 2\pi\eta_d$, where L is the large length scale at which energy is injected into the system and η_d is the small scale at which viscous dissipation becomes significant, energy cascades, à la Richardson [27], from the injection scale L to small length scales of the order of η_d, as large eddies break down into successively smaller daughter eddies. This K41 theory ignores small-scale intermittency, in both spatial and temporal domains; such intermittency appears clearly in experiments and in direct numerical simulations (DNSs) and leads to the multiscaling of structure functions. The characterization of energy spectra and such multiscaling [27] often uses the longitudinal velocity $\mathbf{v}$ structure function $S_p(r) \equiv \langle[\delta v(r)]^p\rangle$, where $\delta v(r) \equiv [\mathbf{v}(\mathbf{x}+\mathbf{r}) - \mathbf{v}(\mathbf{x})] \cdot [\mathbf{r}/r]$, which scales as $S_p(r) \sim r^{\zeta_p}$ for $r \equiv |\,\mathbf{r}\,|$ in the inertial range $\eta_d \ll r \ll L$. The multiscaling exponents ζ_p, which characterize multiscaling, are nonlinear, monotone increasing functions of p [27]. Simple scaling is obtained if ζ_p depends linearly on p, as in the K41 approach [28–30] that yields $\zeta_p^{K41} = p/3$.

Experimental investigations of turbulent flows in liquid helium, in the temperature range between 1.4 and 2.3 K, which covers both the superfluid- and the classical-turbulence regimes, reveal some similarity between ordinary and superfluid turbulence. A Richardson-type cascade leads to a power-law form for $E(k)$ that is consistent with the K41 form; in addition, there are signatures of intermittency, even at temperatures below T_λ [2].

DNSs play an important role in studies of structure-function multiscaling in fluid turbulence [27,31,32]. Such DNSs have achieved impressive spatial resolutions (see, e.g., Refs. [27,31]). By contrast, DNS studies of superfluid turbulence, whether at the level of the Gross-Pitaevskii equation (Refs. [33,34] and references therein) or via the Hall-Vinen-Bekharevich-Khalatnikov (HVBK) equations (Refs. [25,35] and references therein), have only achieved modest spatial

---

[*] Present address: École Normale Supérieure de Lyon, 46 Allée d'Italie, 69007 Lyon, France; research.vishwanath@gmail.com

[†] Also at: Jawaharlal Nehru Centre for Advanced Scientific Research, Jakkur, Bangalore, India; rahul@physics.iisc.ernet.in

resolutions. Furthermore, the large number of parameters in these equations, e.g., the mutual-friction coefficients, the ratio of the normal-fluid density to the superfluid density, and the Reynolds number, pose a significant challenge for systematic studies of the multiscaling of normal-fluid- and superfluid-velocity structure functions. It has been suggested, therefore, that shell models for the 3D-HVBK equations [36–38] be used first to study such multiscaling in detail.

Ever since their introduction in the early work of Obukhov [39], Desnyansky and Novikov [40], and Gledzer, Ohkitani, and Yamada (GOY) [41,42], shell models have played valuable roles in elucidating the multiscaling properties of structure functions of fluid turbulence [27,43–50]. Over the years, such shell models have been used to study magnetohydrodynamic (MHD) turbulence [51–56], Hall-MHD turbulence [57–60], fluid turbulence with polymer additives [61], fluid turbulence in two dimensions [62], fluid turbulence in dimensions in between two and three [63], turbulence in binary-fluid mixtures [64] and in rotating systems [65], and, as mentioned above, turbulence in superfluids [36–38]. Shell models have also been used to initiate studies of the dynamic multiscaling of time-dependent structure functions [66–68].

We build on the shell-model studies of Refs. [36–38] to explore the dependence of the multiscaling exponents here on the parameters of the 3D-HVBK model. It has been noted in Ref. [38] that, given current computational resources, a systematic study of this parameter dependence lies beyond the scope of a well-resolved DNS of the 3D-HVBK equations; however, such a study is possible if we use shell models for these equations. Our study extends the work of Refs. [36–38] by obtaining a variety of results, which we summarize, before we present the details of our study.

Our study of the 3D-HVBK shell model shows that the multiscaling behavior of the shell-model counterparts of velocity structure functions in superfluid turbulence is more rich than that reported so far [38]. Our calculations show, for the first time, the presence of a temperature range in which inertial-range intermittency is either absent or negligibly small. Moreover, intermittency changes significantly, when we vary the parameters in the HVBK model. We find that, in the limits when the normal-fluid fraction is either small (pure superfluid) or large, the equal-time multiscaling exponents are close to their classical-fluid-turbulence values [38], thus suggesting that the classical-fluid-type intermittency is recovered.

In addition, we find that there are two regions, with intermediate values of the normal-fluid fraction, in which the multiscaling exponents are larger than those observed for the classical-fluid-turbulence or even Kolmogorov's 1941 predictions [27]; between these two regions there is a region in which the multiscaling exponents are close to their K41 values. Therefore, we classify the temperatures below T_λ into different multiscaling regimes in order to systematize the variation of intermittency. We have also investigated the dependence of the multiscaling exponents on the mutual-friction coefficient, with equal proportions of superfluid and normal-fluid components; here, our results show that, for small (weak-coupling limit) and large (strong-coupling limit) values of the mutual-friction coefficient, the multiscaling exponents tend to their classical-fluid-turbulence values, whereas, in an intermediate range, there are deviations from the classical-fluid-turbulence behavior; in particular, the multiscaling exponents are larger than their classical-fluid-turbulence counterparts for high-order structure functions (order $p \geqslant 3$).

The remainder of this paper is organized as follows. In Sec. II we describe the shell model and the numerical methods we use. Section III is devoted to our results. We end with conclusions in Sec. IV.

II. MODELS AND NUMERICAL SIMULATIONS

The simplest form of the incompressible, 3D-HVBK equations [23,35,69] is

$$\rho_s \frac{D\mathbf{u}^s}{Dt} = -\frac{\rho_s}{\rho}\nabla p + \rho_s \sigma \nabla T + \mathbf{F}^s_{mf}, \tag{1a}$$

$$\rho_n \frac{D\mathbf{u}^n}{Dt} = -\frac{\rho_n}{\rho}\nabla p - \rho_n \sigma \nabla T + \mathbf{F}^n_{mf} + \nu_n \nabla^2 \mathbf{u}^n, \tag{1b}$$

with $D\mathbf{u}^i/Dt = \partial \mathbf{u}^i/\partial t + \mathbf{u}^i \cdot \nabla \mathbf{u}^i$, the incompressibility condition $\nabla \cdot \mathbf{u}^i = 0$, and the superscript $i \in (n,s)$ denoting the normal fluid (n) or the superfluid (s); p, σ, and T are the pressure, specific entropy, and temperature, respectively; ρ_n (ρ_s) is the normal-fluid (superfluid) density; and ν_n is the kinematic viscosity of the normal fluid. The mutual-friction terms, which model the interaction between the normal and superfluid components, can be written as $\mathbf{F}^s_{mf} = -(\rho_n/\rho)\mathbf{f}_{mf}$ and $\mathbf{F}^n_{mf} = (\rho_s/\rho)\mathbf{f}_{mf}$ in Eqs. (1a) and (1b), respectively, where

$$\mathbf{f}_{\rm mf} = \frac{B}{2}\frac{\omega_{\rm s}}{|\omega_{\rm s}|} \times (\omega_{\rm s} \times \mathbf{u}_{\rm ns}) + \frac{B'}{2}\omega_{\rm s} \times \mathbf{u}_{\rm ns}, \tag{2}$$

with $\mathbf{u}_{\rm ns} = (\mathbf{u}_{\rm n} - \mathbf{u}_{\rm s})$ the slip velocity and B and B' the coefficients of mutual friction. In most of our studies we set $B' = 0$, so $\mathbf{f}_{\rm mf} = -\frac{B}{2}|\omega_{\rm s}|\mathbf{u}_{\rm ns}$, which is the Gorter-Mellink form [70].

We use the following shell model for the 3D-HVBK equations; it is based on the GOY shell model for a fluid [36],

$$\left[\frac{d}{dt} + \nu_n k_m^2\right] u^n_m = \mathrm{NL}\left[u^n_m\right] + F^n_m + f^n_m, \tag{3}$$

$$\left[\frac{d}{dt} + \nu_s k_m^2\right] u^s_m = \mathrm{NL}\left[u^s_m\right] + F^s_m + f^s_m, \tag{4}$$

where

$$\begin{aligned}\mathrm{NL}[u_m] = \imath[&a k_m u_{m+1} u_{m+2} + b k_{m-1} u_{m-1} u_{m+1}\\ &+ c k_{m-2} u_{m-1} u_{m-2}]^*.\end{aligned} \tag{5}$$

Here, as in the GOY model, we have a logarithmically discretized Fourier space with shell-m wave numbers $k = k_0 \lambda^m$, where $k_0 = 2^{-4}$ and $\lambda = 2$, and kinematic viscosities ν_n and ν_s for the normal fluid and the superfluid, respectively. Of course, ν_s must vanish in a superfluid but, in practical numerical simulations, $\nu_n \gg \nu_s > 0$ for numerical stability. The $*$ denotes complex conjugation. The logarithmic discretization of Fourier space allows us to achieve very high Reynolds numbers, even with a moderate number of shells. In the GOY-shell-model equations, direct interactions are limited to the nearest- and next-nearest-neighbor shells. In contrast, if we write the Navier-Stokes equation in Fourier space, every

Fourier mode of the velocity is directly coupled to every other Fourier mode. The normal and superfluid dynamical variables are, respectively, the complex, scalar, shell velocities $u_m^n(k_m)$ and $u_m^s(k_m)$ and f_m^n and f_m^s are the external forcing terms. The coefficients $a = 1$, $b = -1/2$, and $c = -1/2$ are chosen to conserve the shell-model analogs of energy and helicity in the limit of vanishing viscosity and the absence of external forcing. The shell-model analogs of the mutual-friction terms, which model the interaction between the normal and the superfluid components, are

$$F_m^s = \frac{\rho_n B \Omega_s^{1/2}}{2\rho}\left(u_m^n - u_m^s\right) \tag{6}$$

and

$$F_m^n = -\frac{\rho_s B \Omega_s^{1/2}}{2\rho}\left(u_m^n - u_m^s\right). \tag{7}$$

The shell-model superfluid and normal-fluid enstrophies are, respectively,

$$\Omega_s = \sum_{m=1}^{N} \frac{1}{2} k_m^2 \left|u_m^s\right|^2 \tag{8}$$

and

$$\Omega_n = \sum_{m=1}^{N} \frac{1}{2} k_m^2 \left|u_m^n\right|^2. \tag{9}$$

The total energy is

$$E_T = E_n + E_s \equiv \frac{1}{2} \sum_{m=1}^{N} \left(\left|u_m^n\right|^2 + \left|u_m^s\right|^2\right), \tag{10}$$

where E_n and E_s are the normal-fluid and superfluid energies, respectively. Other statistical quantities that we use in our study are as follows: The helicity is

$$H_i = \sum_{m=1}^{N} \frac{1}{2}\left(\frac{a}{c}\right)^m \frac{\left|u_m^i\right|^2}{k_m}, \tag{11}$$

the energy spectra are

$$E_i(k_m) = \frac{1}{2} \frac{\left|u_m^i\right|^2}{k_m}, \tag{12}$$

the root-mean-square velocities are

$$u_{\mathrm{rms}}^i = \left(\sum_m \left|u_m^i\right|^2\right)^{1/2}, \tag{13}$$

the Taylor microscale is

$$\lambda_i = \left[\frac{\sum_m E^i(k_m)}{\sum_m k_m^2 E^i(k_m)}\right]^{1/2}, \tag{14}$$

the Taylor-microscale Reynolds number is

$$\mathrm{Re}_\lambda^i = u_{\mathrm{rms}} \lambda_i / \nu_i, \tag{15}$$

the integral length scale is

$$\ell_I = \frac{\sum_m E^i(k_m)/k_m}{\sum_m E^i(k_m)}, \tag{16}$$

and the large-eddy-turnover time is

$$T_{\mathrm{eddy}}^i = \frac{1}{k_1 u_1^i}, \tag{17}$$

and here and henceforth $i \in (n,s)$.

The equal-time, order-p structure functions for the shell model are

$$S_p^i(k_m) \equiv \left\langle \left[u_m^i(t) u_m^{i*}(t)\right]^{p/2} \right\rangle \sim k_m^{-\zeta_p^i}, \tag{18}$$

where the power-law dependence is obtained only if k_m^{-1} lies in the inertial range. The structure functions defined above show period-three oscillations because of three cycles in the static solutions of the GOY model for the Navier-Stokes equation [45]. Therefore, we use the modified structure functions [44,45]

$$\Sigma_p^i \equiv \left\langle \left|\mathrm{Im}\left[u_{m+2}^i u_{m+1}^i u_m^i - \tfrac{1}{4} u_{m-1}^i u_m^i u_{m+1}^i\right]\right|^{p/3} \right\rangle \sim k_m^{-\zeta_p^i}, \tag{19}$$

which filter out these oscillations effectively. The Sabra-model variant [37,38] of the 3D-HVBK equations does not show such oscillations. We expect that the multiscaling exponents ζ_p^i, $i \in (n,s)$, satisfy the following convexity inequality for any three positive integers $p_1 \leqslant p_2 \leqslant p_3$ [27]:

$$(p_3 - p_1)\zeta_{2p_2}^i \geqslant (p_3 - p_2)\zeta_{2p_1}^i + (p_2 - p_1)\zeta_{2p_3}^i. \tag{20}$$

We obtain smooth energy spectra, without period-3 oscillations, by using $E_i(k_m) = \Sigma_2^i(k_m)/k_m$, $i \in (n,s)$.

To obtain a turbulent, but statistically steady, state, we force both the superfluid and the normal-fluid components with the forces

$$f_m^{n,s} = (1 + \imath) \times 5 \times 10^{-3} \delta_{1,m}, \tag{21}$$

where $\delta_{1,m}$ is the Kronecker δ. We use the second-order, slaved Adams-Bashforth scheme to integrate the 3D-HVBK shell-model Eqs. (3) and (4) [44,71]. To study the multiscaling behaviors of structure functions here, we design the following three sets of runs:

(1) `G1–G21`: In these runs, we use the values of ρ_n/ρ and B, which have been measured at different temperatures in experiments on helium II [72,73]; we list them, along with other parameters, in Table I. We use $\nu_n = 10^{-9}$, $\nu_s = 10^{-11}$ and the time step $\Delta t = 10^{-6}$.

(2) `B1–B19`: We vary ρ_n/ρ between 0.05 and 0.95 and keep $B = 1.5$ fixed.

(3) `R1–R12`: We vary B between 0.1 and 10 and keep $\rho_n/\rho = 0.5$ fixed.

In the runs `B1–B19` and `R1–R12`, we use $\nu_n = 10^{-7}$, $\nu_s = 10^{-9}$, and the time step $\Delta t = 10^{-5}$.

We use the initial condition $u_m^{n,s} = (1 + \imath) k_m e^{-k_m^2}$, for $1 \leqslant m \leqslant N$, in the run `PG`. In the runs `G1–G21`, `B1–B19`, and `R1–R12`, we use the initial values $u_m^{n,s} = u_0^{n,s} k_m^{1/2} e^{-k_m^2} e^{i\vartheta_m}$, for $1 \leqslant m \leqslant N$, where ϑ_m is a random phase distributed uniformly on $[0,2\pi)$. We include the GOY-shell-model run `PG` ($\nu_n = 10^{-9}$) for the purpose of comparison with the runs `G1–G21`. We use the boundary conditions $u_{-2}^i = u_{-1}^i = u_0^i = 0$ and $u_{N+1}^i = u_{N+2}^i = 0$, $i \in (n,s)$. We report results for $N = 36$ shells; Ref. [36] uses $N = 18$ and Ref. [38] presents data with $N = 36$.

TABLE I. Parameters for our 3D shell-model run (classical-fluid-turbulence) `PG` and 3D-HVBK shell-model runs `G1`–`G21`: T is the temperature, ρ_n/ρ is the normal-fluid density fraction, and B is the mutual-friction coefficient. λ_n (λ_s) is the Taylor microscale for the normal-fluid (superfluid); Re_λ^n (Re_λ^s) is the Taylor-microscale Reynolds number for the normal-fluid (superfluid). For the runs `G1`–`G21` we obtain statistical quantities by averaging in time over 439 T_{eddy}, where the large-eddy-turnover time for the normal fluid (superfluid) is $T_{\mathrm{eddy}}^n \simeq 22.80$ ($T_{\mathrm{eddy}}^s \simeq 22.80$).

	$T(K)$	ρ_n/ρ	B	λ_n	λ_s	$(10^8)\ \mathrm{Re}_\lambda^n$	$(10^{10})\ \mathrm{Re}_\lambda^s$
PG				0.50		3.1	
G1	1.60	0.162	1.193	0.28	0.21	3.2	2.4
G2	1.65	0.193	1.144	0.29	0.22	3.2	2.4
G3	1.70	0.229	1.100	0.29	0.22	3.3	2.5
G4	1.75	0.268	1.059	0.30	0.22	3.3	2.5
G5	1.80	0.313	1.024	0.31	0.23	3.4	2.6
G6	1.85	0.364	0.996	0.26	0.20	2.9	2.2
G7	1.90	0.420	0.980	0.29	0.23	3.3	2.5
G8	1.95	0.482	0.981	0.30	0.24	3.4	2.6
G9	2.00	0.553	1.008	0.29	0.23	3.3	2.6
G10	2.02	0.595	1.04	0.28	0.23	3.2	2.6
G11	2.04	0.629	1.07	0.28	0.23	3.1	2.6
G12	2.06	0.666	1.13	0.27	0.23	3.1	2.6
G13	2.08	0.705	1.21	0.27	0.23	3.0	2.6
G14	2.10	0.741	1.298	0.27	0.23	3.0	2.6
G15	2.12	0.788	1.476	0.27	0.23	3.0	2.7
G16	2.14	0.842	1.790	0.27	0.24	3.0	2.7
G17	2.16	0.907	2.420	0.27	0.25	3.1	2.8
G18	2.170	0.950	3.154	0.27	0.26	3.1	2.9
G19	2.172	0.961	3.538	0.27	0.26	3.1	2.9
G20	2.174	0.973	4.227	0.28	0.26	3.1	3.0
G21	2.176	0.988	6.391	0.28	0.27	3.1	3.0

III. RESULTS

We now present the results of our study of superfluid and normal-fluid turbulence in the 3D-HVBK shell model. We begin with energy spectra and then examine the parameter dependence of the exponents that characterize the multiscaling of structure functions.

In Table I we list the values of λ_i, Re_λ^i, and T_{eddy}^i that we obtain from our 3D classical-fluid-turbulence and HVBK shell-model simulations `PG` and `G1`–`G21`, respectively. Figure 1 compares $E_n(k_m)$ (full curves) and $E_s(k_m)$ (dashed curves), compensated by $k^{5/3}$, for four representative values of ρ_n/ρ [runs `G1` (purple curves with +), `G7` (green curves with circles), `G14` (sky-blue curves with $*$), and `G21` (brown curves with ×)]. The inertial ranges of $E_n(k_m)$ and $E_s(k_m)$ exhibit scaling that is consistent with a $k^{-5/3}$ power-law form (orange dashed line); of course, this exponent is not exactly $-5/3$ if the structure functions display multiscaling. The run `PG` (yellow curve with squares) shows the energy spectrum for classical fluid turbulence. The coupling between the normal and superfluid components modifies the classical-fluid energy spectrum; the spectra for the two components, in the inertial range lie on top of each other; and, in the dissipation range, $E_n(k_m)$ is pulled up towards $E_s(k_m)$ by virtue of the mutual-friction-induced tendency of locking between u_n and u_s (see Ref. [25]).

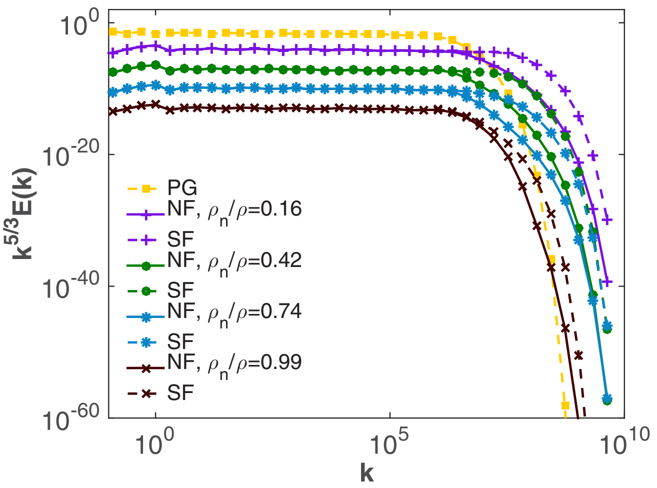

FIG. 1. Log-log (base 10) plots of the spectra $E_n(k_m)$ (full curves) and $E_s(k_m)$ (dashed curves), compensated by $k^{5/3}$, from our shell-model runs: `PG` (yellow curves); `G1` (purple curves); `G7` (green curves); `G14` (sky-blue curves); `G21` (brown curves); and NF (SF) stands for normal-fluid (superfluid). We have shifted these spectra, relative to each other, so spectra for different values of ρ_n/ρ are separated clearly from each other; we do so by multiplying the spectrum for run `G1` by 10^{-3} for run `G7` by 10^{-6}, for run `G14` by 10^{-9}, and for run `G21` by 10^{-12}.

We study the multiscaling behaviors of the velocity structure functions for the 3D-HVBK shell model by calculating the multiscaling exponents ζ_p^n and ζ_p^s, for the normal fluid and superfluid components, respectively, by using the Eqs. (19) for Σ_p^i. In Table I in the Supplemental Material [74], we list the values of these exponents, which we have obtained from Σ_p^i, for $p = 1$ to 6, $i \in (n,s)$. Each row of this table has two lines; the first and second lines contain, respectively, the values of ζ_p^n and ζ_p^s. Table I in the Supplemental Material [74] shows that $\zeta_p^n = \zeta_p^s$, for $p = 1$ to 6, for the runs `G1`–`G21`, because of the mutual-friction-induced locking of the normal fluid and superfluid velocities in the inertial range.

In Fig. 2 we show the plots of ζ_p^n versus the order p for various values of ρ_n/ρ; the analogous plots for the superfluid component are similar because of the locking between the two components. The orange solid line is the K41 prediction $\zeta_p^{K41} = p/3$, and the purple solid line shows the multiscaling exponents ζ_p^c for classical (superscript c), 3D fluid turbulence. The multiscaling exponents ζ_p^i, $i \in (n,s)$, which we determine from the 3D-HVBK shell model, show deviations from ζ_p^c; these deviations depend on the values of ρ_n/ρ and B. For the run with $\rho_n/\rho = 0.27$ and $B = 1.059$ at $T = 1.75\,K$, the ζ_p^n's (green dashed line in Fig. 2) lie roughly between ζ_p^{K41} and ζ_p^c. We obtain similar results for the cases $\rho_n/\rho = 0.55$ and $\rho_n/\rho = 0.71$; however, the differences among ζ_p^n and ζ_p^{K41} and ζ_p^c depend on p. Moreover, for the run with $\rho_n/\rho = 0.36$ and $B = 0.996$ at $T = 1.85\,K$, the ζ_p^n's (light blue dot-dashed line in Fig. 2) is close to $\zeta_p^{K41} = p/3$. The run with $\rho_n/\rho = 0.91$ and $B = 2.42$ at $T = 2.16\,K$ (magenta dotted line with circles) the ζ_p^n's lie almost on top of ζ_p^c (purple solid line).

To understand the dependence of the multiscaling exponents ζ_p^i, $i \in (n,s)$, on ρ_n/ρ (which includes the variation

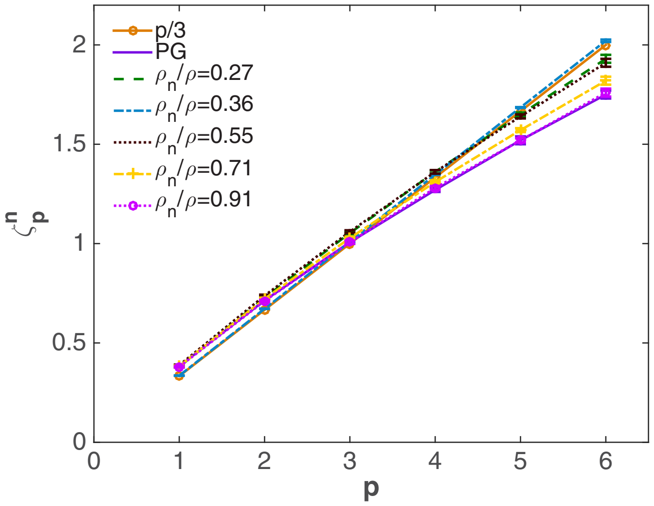

FIG. 2. Plots versus order p of the multiscaling exponents: ζ_p^n for the shell-model runs `G4` (green curve), `G6` (sky-blue curve), `G9` (brown curve), `G13` (yellow curve), and `G17` (magenta curve). `PG` is the classical-fluid-turbulence run (purple curve) and $\zeta^{K41} = p/3$ is denoted by the orange line.

of B with temperature), we plot, in Fig. 3, ζ_p^n, for $p = 1$ to 6, versus ρ_n/ρ from our runs `G1`–`G21`. Figure 3 shows that, depending on the values of ρ_n/ρ, the behavior of the exponents ζ_p^n can be classified *roughly* into the following six regions I–V (demarcated by gray dashed vertical lines on the plot). Region I ($\rho_n/\rho \lesssim 0.175$): The values of ζ_p^n are close to the classical-fluid-turbulence exponents ζ_p^c. Region II ($0.175 < \rho_n/\rho < 0.3$): $\zeta_p^n > \zeta_p^c$, for $p \geqslant 3$ and, for $p = 1,2$, $\zeta_p^n \simeq \zeta_p^c$. Region III ($0.32 \lesssim \rho_n/\rho \lesssim 0.4$): a narrow region for which $\zeta_p^n \simeq \zeta_p^{K41}$. Region IV ($0.4 < \rho_n/\rho \lesssim 0.65$): ζ_p^n show significant deviations from both ζ_p^c and ζ_p^{K41}. Region V ($0.65 < \rho_n/\rho < 0.75$): ζ_p^n shows a tendency to move towards ζ_n^c. Region VI ($\rho_n/\rho \gtrsim 0.75$): $\zeta_p^n \simeq \zeta_p^c$.

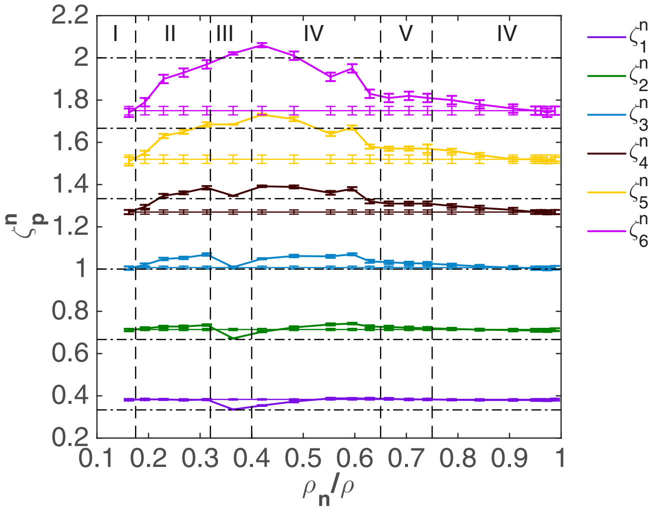

FIG. 3. Plots of ζ_p^n, for $p = 1$ to 6, versus ρ_n/ρ, from our shell-model runs `G1`–`G21`. For reference, we show the value of the classical-fluid-turbulence exponent ζ_p^c, for order p, by a horizontal, dashed line; different colors indicate different values of the order p. The black dot-dashed lines indicates $\zeta_p^{K41} = p/3$.

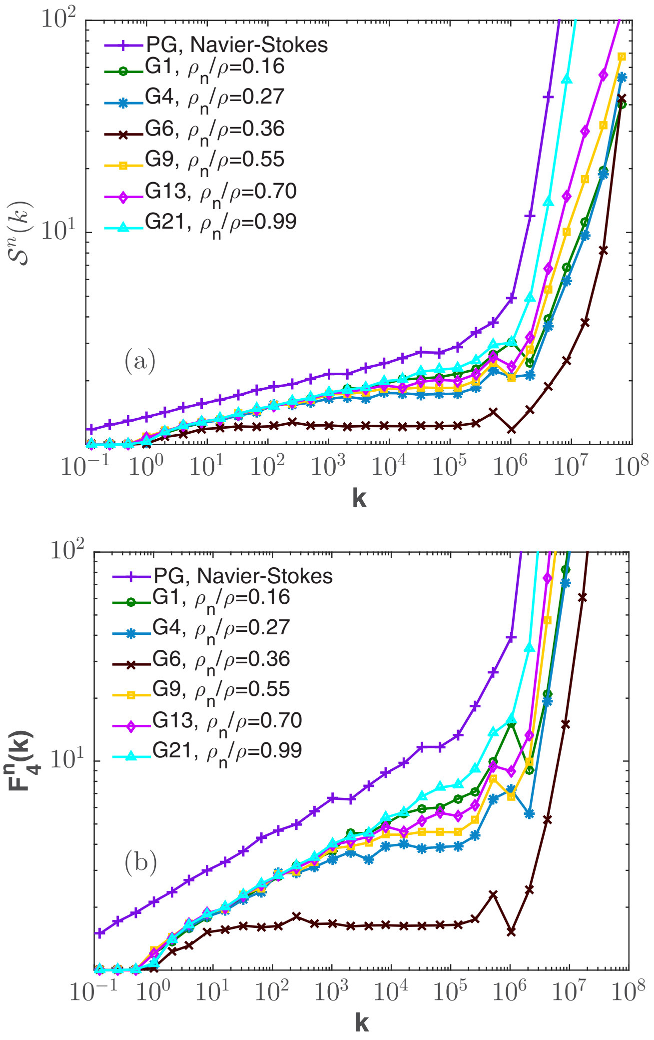

FIG. 4. Log-log plots of (a) the skewness $\mathcal{S}_i$ and (b) the flatness $F_4^i, i \in (n,s)$, for our shell-model runs `G1` ($\rho_n/\rho = 0.16$), `G4` ($\rho_n/\rho = 0.27$), `G6` ($\rho_n/\rho = 0.36$), `G9` ($\rho_n/\rho = 0.55$), `G13` ($\rho_n/\rho = 0.70$), and `G21` ($\rho_n/\rho = 0.99$) for the six regions identified in Fig. 3. `PG` is our classical-fluid-turbulence run.

In Fig. 4 we plot [Fig. 4(a)] the skewness factor $\mathcal{S}_i = \Sigma_3^i(k)/[\Sigma_2^i(k)]^{3/2}$ and [Fig. 4(b)] the flatness factor $F_4^i = \Sigma_4^i(k)/[\Sigma_2^i(k)]^2$, $i \in (n,s)$, for six different values of ρ_n/ρ in the six regions identified above. For $\rho_n/\rho = 0.36$, both $\mathcal{S}^n(k)$ [Fig. 4(a)] and $F_4^n(k)$ [Fig. 4(b)] show a clear k-independent plateau region, thereby providing strong proof that, in the range $0.32 \lesssim \rho_n/\rho \lesssim 0.4$, the multiscaling exponents of the Σ structure functions are close to their K41 values. This behavior indicates the presence of a temperature range (region III in Fig. 3) for superfluid helium in which inertial-range intermittency is either absent or negligibly small; however, it is also evident from the apparent similarity of $F_4^n(k)$, computed for the runs `G1` (green curve with circles) and `G21` (cyan curve with triangles) with those for run `PG` (the Navier-Stokes-GOY shell model) in Fig. 4 that, in the temperature ranges corresponding to regions I and VI,

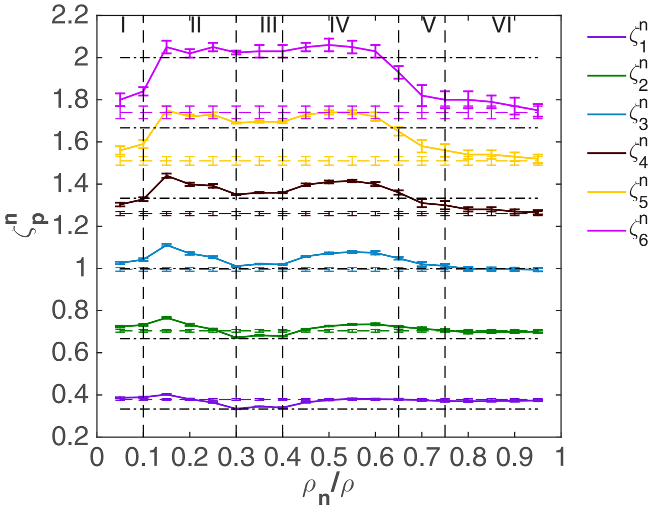

FIG. 5. Plots of ζ_p^n, for $p = 1$ to 6, versus ρ_n/ρ, from our shell-model runs B1–B19. For reference, we show the value of the classical-fluid-turbulence exponent ζ_p^c by a horizontal dashed line; different colors indicate different values of the order p. The black, dot-dashed lines indicates $\zeta_p^{K41} = p/3$. In the shell-model runs B1–B19, we keep the mutual-friction coefficient fixed at $B = 1.5$.

classical-fluid-type intermittency is recovered. It is interesting to note the flattening of $F_4^n(k)$, towards the high-k end of the inertial range, for the runs G4 (blue cure with asterisks), in region II, and G9 (yellow curve with squares), in region IV; here, ζ_p^n show significant deviations from both ζ_p^c and ζ_p^{K41}. The flatness $F_n^i(k)$ (or its variant that can be computed by using a high-pass filter on the velocity signal [27,61]) also exhibits significant growth at large wave numbers for all the cases we have studied; this signifies the presence of strong intermittency at small length scales.

We now examine the dependence of the multiscaling exponents $\zeta_p^i, i \in (n,s)$, on ρ_n/ρ, while keeping the coefficient of mutual friction $B = 1.5$ fixed, in runs B1–B19. These runs allow us to classify the behavior of ζ_p^i, $i \in (n,s)$, as a function of ρ_n/ρ, more clearly than the runs G1–G21. In Table II in the Supplemental Material [74], we list the values of ζ_p^i, $i \in (n,s)$, which we extract from Σ_p^i [Eq. (19)], for $p = 1$ to 6, $i \in (n,s)$. Each row of this table has two lines; the first and second lines contain the values of ζ_p^n and ζ_p^s, respectively. For these runs $\zeta_p^n \simeq \zeta_p^s$. In Fig. 5 we plot ζ_p^n versus ρ_n/ρ for $p = 1$ to 6 in runs B1–B19. These plots show two regions ($0.1 < \rho_n/\rho < 0.3$ and $0.4 < \rho_n/\rho < 0.65$) with clear bumps, where the values of ζ_p^n deviate significantly from both $\zeta_p^{K41}(< \zeta_p^n)$ and $\zeta_p^c(< \zeta_p^n)$. We classify *roughly* the behaviors

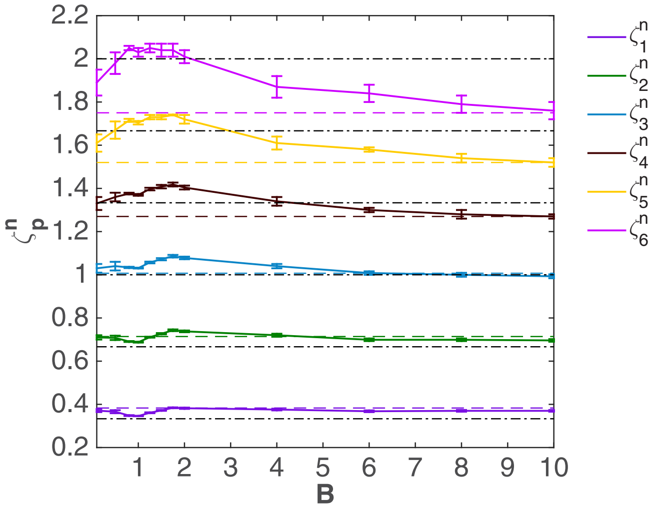

FIG. 6. Plot of ζ_p^n, for $p = 1$ to 6, versus ρ_n/ρ, from the shell-model runs R1–R12. For reference, we show the value of the classical-fluid-turbulence exponent ζ_p^c by a horizontal dashed line; different colors indicate different values of the order p. The black, dot-dashed lines indicates $\zeta_p^{K41} = p/3$. In the shell-model runs R1–R12, we keep the normal-fluid density fraction fixed at $\rho_n/\rho = 0.5$.

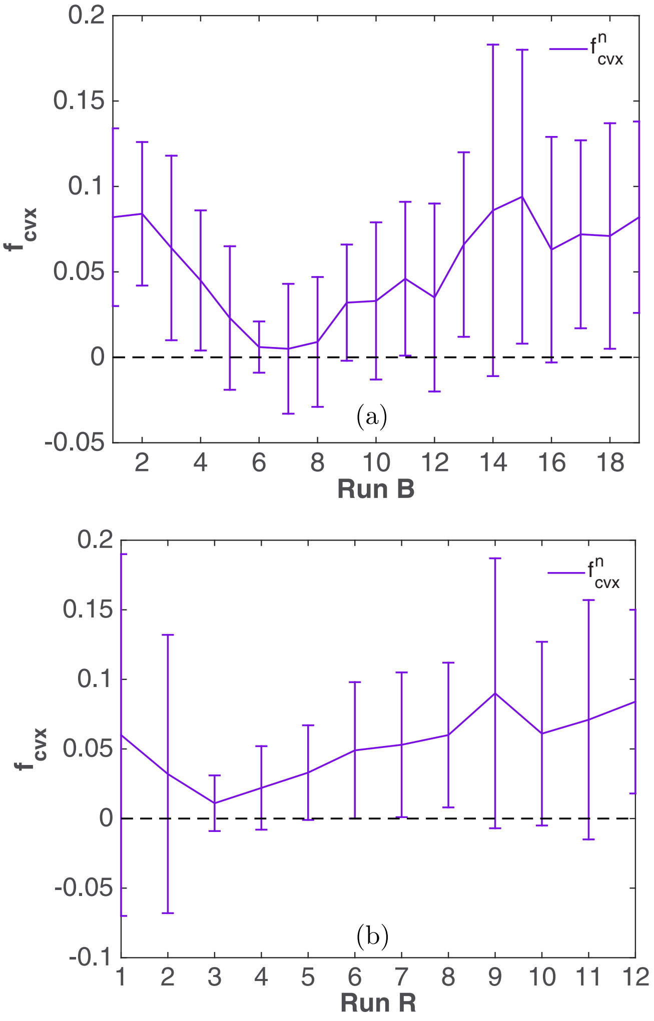

FIG. 7. Plots of (a) $f^n_{\rm cvx}$ for the runs B1–B19 ($B = 1.5$) and (b) $f^n_{\rm cvx}$ for the runs R1–R12 ($\rho_n/\rho = 0.5$), where $f^i_{\rm cvx} = (p_3 - p_1)\zeta^i_{2p_2} - (p_3 - p_2)\zeta^i_{2p_1} - (p_2 - p_1)\zeta^i_{2p_3}$, $i \in (n,s)$, and we take $p_1 = 1$, $p_2 = 2$, and $p_3 = 3$. The multiscaling exponents ζ_p^i, $i \in (n,s)$, satisfy the convexity constraint, if $f^i_{\rm cvx} > 0$, for any three positive integers $p_1 \leqslant p_2 \leqslant p_3$. The x-axis label in the above plots indicates the run index, e.g., B1.

of these ζ_p^n into six regions I–VI (demarcated by gray dashed vertical lines in Fig. 5), which we describe below. Region I ($\rho_n/\rho \lesssim 0.1$): $\zeta_p^n \simeq \zeta_p^c$. Region II ($0.1 < \rho_n/\rho < 0.3$): ζ_p^n differs significantly from both ζ_p^c and ζ_p^{K41}, with $\zeta_p^c < \zeta_p^n$ and $\zeta_p^{K41} < \zeta_p^n$. Region III ($0.3 \lesssim \rho_n/\rho \lesssim 0.4$): $\zeta_p^n \simeq \zeta_p^{K41}$. Region IV ($0.4 < \rho_n/\rho < 0.65$): ζ_p^n differs significantly from both ζ_p^c and ζ_p^{K41}, with $\zeta_p^c < \zeta_p^n$ and $\zeta_p^{K41} < \zeta_p^n$. Region V ($0.65 \gtrsim \rho_n/\rho < 0.75$): ζ_p^n shows a tendency to move towards ζ_n^c. Region VI ($\rho_n/\rho \gtrsim 0.75$): $\zeta_p^n \simeq \zeta_p^c$.

We also explore the dependence of the multiscaling exponents ζ_p^i, $i \in (n,s)$, on the mutual-friction coefficient B, while keeping the normal-fluid-density fraction $\rho_n/\rho = 0.5$ fixed. In our 3D-HVBK shell-model runs `R1`–`R12`, we systematically vary the values of B; we list the values of ζ_p^i, $i \in (n,s)$ obtained from Σ_p^i [Eq. (19)], for $p = 1$ to 6, in Table III in the Supplemental Material [74]. Each row of this table has two lines; the first and second lines contain, respectively, the values of ζ_p^n and ζ_p^s. In Fig. 6 we plot ζ_p^n versus B, for $p = 1$ to 6, for the runs `R1`–`R12`; the exponents ζ_p^n deviate significantly from their classical-fluid-turbulence counterparts ζ_p^c, in the range $1 \leqslant B \leqslant 3$, with $\zeta_p^n > \zeta_p^c$, for $p \geqslant 3$, $\zeta_1^n < \zeta_1^c$, and ζ_2^n marginally larger than ζ_2^c. As $B \to 0.1$ (small values) and $B \to 10$ (large values) the multiscaling exponents $\zeta_p^n \simeq \zeta_p^c$, because, in the limit $B \to 0$, the normal fluid and superfluid are uncoupled, and for very large values of B, the coupling is so strong that single-fluid-turbulence results emerge.

We have checked explicitly that all the values of ζ_p^n and ζ_p^s, which we have reported above, satisfy the convexity inequality Eq. (20). We illustrate this in the plots of Fig. 7.

IV. CONCLUSIONS

We have carried out extensive numerical simulations of the 3D-HVBK shell model, specifically to study the multiscaling of structure functions in superfluid turbulence, because such multiscaling has been studied much less than its counterpart in classical-fluid turbulence. Experimental investigations of turbulence in liquid helium, below the superfluid transition temperature T_λ, have provided evidence for multiscaling, in the inertial range [2,9,75]. These experiments have also motivated our study. Direct numerical simulations of models for superfluids, e.g., the Gross-Pitaevskii equation and the HVBK two-fluid equations, have not been able to cover the large range of length scales that are required to obtain reliable data for high-order structure functions. Shell models, based on the HVBK two-fluid equations, have been used to study the statistical properties of 3D superfluid turbulence in both ^{4}He [36,38] and ^{3}He-B [36,37]; these studies have elucidated the natures of energy spectra and fluxes for both forced statistically steady and decaying superfluid turbulence. The only detailed investigation of the multiscaling behavior of structure functions here is an HVBK shell-model study [38]. This study has shown that, for $\rho_n/\rho \leqslant 0.1$ and $\rho_n/\rho \geqslant 0.9$, the multiscaling exponents are close to those in classical-fluid turbulence; whereas, in the range $0.25 \leqslant \rho_n/\rho \leqslant 0.5$, high-order multiscaling exponents deviate significantly from, and are smaller than, their classical-fluid-turbulence counterparts.

Our detailed study of the 3D-HVBK shell model has shown that the multiscaling of structure functions in superfluid turbulence is more complex than that reported in Ref. [38]. However, our results agree with those of Ref. [38] in that, for $\rho_n/\rho \lesssim 0.1$ and $\rho_n/\rho \gtrsim 0.75$, the multiscaling exponents are close to the classical-fluid-turbulence values. Moreover, we find that there are two regions, with $0.1 < \rho_n/\rho < 0.3$ and $0.4 < \rho_n/\rho < 0.65$, where the multiscaling exponents are larger than their classical-fluid-turbulence and K41 counterparts, i.e., $\zeta_p^i > \zeta_p^c$ and $\zeta_p^i > \zeta_p^{K41}$, $i \in (n,s)$. In the range $0.3 \lesssim \rho_n/\rho \lesssim 0.4$, these exponents are close to the K41 prediction, i.e., $\zeta_p^i \simeq \zeta_p^{K41}$. We have also investigated the dependence of the multiscaling exponents on the mutual-friction coefficient B, with $\rho_n/\rho = 0.5$ fixed; our results show that, for small (weak-coupling limit) and large (strong-coupling limit) values of B, the multiscaling exponents tend to their classical-fluid-turbulence values, whereas, in the range $1 \lesssim B \lesssim 3$, there are deviations from the classical-fluid-turbulence behavior $\zeta_p^i > \zeta_p^c$ for $p \geqslant 3$. We hope our extensive study of the multiscaling of structure functions in the 3D-HVBK shell model will stimulate detailed experimental and DNS studies of such multiscaling in quantum-fluid turbulence in different quantum fluids.

ACKNOWLEDGMENTS

We thank CSIR, UGC, DST (India), and the Indo-French Centre for Applied Mathematics (IFCAM) for financial support and SERC (IISc) for computational resources. V.S. acknowledges support from Centre Franco-Indien pour la Promotion de la Recherche Avancée (CEFIPRA/IFCPAR) Project No. 4904. We are grateful to A. Basu and S. S. Ray for useful discussions. We acknowledge the improvements suggested by the anonymous reviewers.

---

[1] M. R. Smith, R. J. Donnelly, N. Goldenfeld, and W. F. Vinen, Phys. Rev. Lett. **71**, 2583 (1993).

[2] J. Maurer and P. Tabeling, Europhys. Lett. **43**, 29 (1998).

[3] S. R. Stalp, L. Skrbek, and R. J. Donnelly, Phys. Rev. Lett. **82**, 4831 (1999).

[4] L. Skrbek, J. J. Niemela, and R. J. Donnelly, Phys. Rev. Lett. **85**, 2973 (2000).

[5] T. Zhang and S. W. Van Sciver, Nat. Phys. **1**, 36 (2005).

[6] G. P. Bewley, D. P. Lathrop, and K. R. Sreenivasan, Nature **441**, 588 (2006).

[7] P.-E. Roche, P. Diribarne, T. Didelot, O. Français, L. Rousseau, and H. Willaime, Europhys. Lett. **77**, 66002 (2007).

[8] E. A. L. Henn, J. A. Seman, G. Roati, K. M. F. Magalhães, and V. S. Bagnato, Phys. Rev. Lett. **103**, 045301 (2009).

[9] J. Salort, B. Chabaud, E. Lévêque, and P.-E. Roche, Europhys. Lett. **97**, 34006 (2012).

[10] D. E. Zmeev, F. Pakpour, P. M. Walmsley, A. I. Golov, W. Guo, D. N. McKinsey, G. G. Ihas, P. V. E. McClintock, S. N. Fisher, and W. F. Vinen, Phys. Rev. Lett. **110**, 175303 (2013).

[11] T. W. Neely, A. S. Bradley, E. C. Samson, S. J. Rooney, E. M. Wright, K. J. H. Law, R. Carretero-González, P. G. Kevrekidis, M. J. Davis, and B. P. Anderson, Phys. Rev. Lett. **111**, 235301 (2013).
[12] M. S. Paoletti and D. P. Lathrop, Annu. Rev. Condens. Matter Phys. **2**, 213 (2011).
[13] L. Skrbek and K. R. Sreenivasan, Phys. Fluids **24**, 011301 (2012).
[14] G. V. Kolmakov, P. V. E. McClintock, and S. V. Nazarenko, Proc. Natl. Acad. Sci. USA **111**, 4727 (2014).
[15] N. G. Berloff, M. Brachet, and N. P. Proukakis, Proc. Natl. Acad. Sci. USA **111**, 4675 (2014).
[16] C. F. Barenghi, V. S. Lvov, and P.-E. Roche, Proc. Natl. Acad. Sci. USA **111**, 4683 (2014).
[17] R. Hänninen and A. W. Baggaley, Proc. Natl. Acad. Sci. USA **111**, 4667 (2014).
[18] C. Nore, M. Abid, and M. E. Brachet, Phys. Rev. Lett. **78**, 3896 (1997).
[19] K. W. Schwarz, Phys. Rev. B **18**, 245 (1978).
[20] K. W. Schwarz, Phys. Rev. B **31**, 5782 (1985).
[21] K. W. Schwarz, Phys. Rev. B **38**, 2398 (1988).
[22] I. M. Khalatnikov, *An Introduction to the Theory of Superfluidity* (W.A. Benjamin, New York, 1965).
[23] P.-E. Roche, C. F. Barenghi, and E. Lévêque, Europhys. Lett. **87**, 54006 (2009).
[24] C. F. Barenghi, Phys. Rev. B **45**, 2290 (1992).
[25] V. Shukla, A. Gupta, and R. Pandit, Phys. Rev. B **92**, 104510 (2015).
[26] M. S. Paoletti, M. E. Fisher, K. R. Sreenivasan, and D. P. Lathrop, Phys. Rev. Lett. **101**, 154501 (2008).
[27] U. Frisch, *Turbulence* (Cambridge University Press, Cambridge, UK, 1996), Vol. 1.
[28] A. N. Kolmogorov, Dokl. Akad. Nauk SSSR **30**, 301 (1941).
[29] A. N. Kolmogorov, Dokl. Akad. Nauk SSSR **31**, 538 (1941).
[30] A. N. Kolmogorov, Dokl. Akad. Nauk SSSR **32**, 16 (1941).
[31] T. Ishihara, T. Gotoh, and Y. Kaneda, Annu. Rev. Fluid Mech. **41**, 165 (2009).
[32] A. Arnèodo *et al.* (International Collaboration for Turbulence Research), Phys. Rev. Lett. **100**, 254504 (2008).
[33] V. Shukla, M. Brachet, and R. Pandit, New J. Phys. **15**, 113025 (2013).
[34] V. Shukla, M. Brachet, and R. Pandit, arXiv:1412.0706.
[35] V. Shukla, Particles and fields in superfluid turbulence: Numerical and theoretical studies, Ph.D. thesis, Indian Institute of Science, Bangalore, 2014.
[36] D. H. Wacks and C. F. Barenghi, Phys. Rev. B **84**, 184505 (2011).
[37] L. Boué, V. L'vov, A. Pomyalov, and I. Procaccia, Phys. Rev. B **85**, 104502 (2012).
[38] L. Boué, V. L'vov, A. Pomyalov, and I. Procaccia, Phys. Rev. Lett. **110**, 014502 (2013).
[39] A. M. Obukhov, Atmos. Oceanic Phys. **10**, 127 (1974).
[40] V. N. Desnyansky and E. A. Novikov, Prikl. Mat. Mekh. **38**, 507 (1974).
[41] E. B. Gledzer, Sov. Phys. Dokl. SSSR **18**, 216 (1973).
[42] K. Ohkitani and M. Yamada, Prog. Theor. Phys. **81**, 329 (1982).
[43] M. H. Jensen, G. Paladin, and A. Vulpiani, Phys. Rev. A **43**, 798 (1991).
[44] D. Pisarenko, L. Biferale, D. Courvoisier, U. Frisch, and M. Vergassola, Phys. Fluids A **5**, 2533 (1993).
[45] S. Dhar, A. Sain, A. Pande, and R. Pandit, Pramana J. Phys. **48**, 325 (1997).
[46] S. K. Dhar, A. Sain, and R. Pandit, Phys. Rev. Lett. **78**, 2964 (1997).
[47] L. Biferale, Annu. Rev. Fluid Mech. **35**, 441 (2003).
[48] T. Bohr, M. H. Jensen, G. Paladin, and A. Vulpiani, *Dynamical Systems Approach to Turbulence*, Cambridge Nonlinear Science Series (Cambridge University Press, Cambridge, UK, 2005).
[49] P. D. Ditlevsen, *Turbulence and Shell Models* (Cambridge University Press, Cambridge, UK, 2010).
[50] V. S. L'vov, E. Podivilov, A. Pomyalov, I. Procaccia, and D. Vandembroucq, Phys. Rev. E **58**, 1811 (1998).
[51] A. Basu, A. Sain, S. K. Dhar, and R. Pandit, Phys. Rev. Lett. **81**, 2687 (1998).
[52] C. Kalelkar and R. Pandit, Phys. Rev. E **69**, 046304 (2004).
[53] G. Sahoo, D. Mitra, and R. Pandit, Phys. Rev. E **81**, 036317 (2010).
[54] P. Frick and D. Sokoloff, Phys. Rev. E **57**, 4155 (1998).
[55] A. Brandenburg, K. Enqvist, and P. Olesen, Phys. Rev. D **54**, 1291 (1996).
[56] P. Giuliani and V. Carbone, Europhys. Lett. **43**, 527 (1998).
[57] D. Hori, M. Furukawa, S. Ohsaki, and Z. Yoshida, J. Plasma Fusion Res. **81**, 141 (2005).
[58] D. Hori and H. Miura, J. Plasma Fusion Res. **3**, S1053 (2008).
[59] S. Galtier, Phys. Rev. E **77**, 015302 (2008).
[60] D. Banerjee, S. S. Ray, G. Sahoo, and R. Pandit, Phys. Rev. Lett. **111**, 174501 (2013).
[61] C. Kalelkar, R. Govindarajan, and R. Pandit, Phys. Rev. E **72**, 017301 (2005).
[62] E. Aurell, G. Boffetta, A. Crisanti, P. Frick, G. Paladin, and A. Vulpiani, Phys. Rev. E **50**, 4705 (1994).
[63] P. Giuliani, M. H. Jensen, and V. Yakhot, Phys. Rev. E **65**, 036305 (2002).
[64] S. S. Ray and A. Basu, Phys. Rev. E **84**, 036316 (2011).
[65] Y. Hattori, R. Rubinstein, and A. Ishizawa, Phys. Rev. E **70**, 046311 (2004).
[66] D. Mitra and R. Pandit, Phys. Rev. Lett. **93**, 024501 (2004).
[67] D. Mitra, S. S. Ray, and R. Pandit, Eur. Phys. J. B **64**, 463 (2008).
[68] S. S. Ray, D. Mitra, and R. Pandit, New J. Phys. **10**, 033003 (2008).
[69] R. J. Donnelly, *Quantized Vortices in Helium II* (Cambridge University Press, Cambridge, 1991), Vol. 2.
[70] C. J. Gorter and J. H. Mellink, Physica **15**, 285 (1949).
[71] S. M. Cox and P. C. Matthews, J. Comput. Phys. **176**, 430 (2002).
[72] R. J. Donnelly and C. F. Barenghi, J. Phys. Chem. Ref. Data **27**, 1217 (1998).
[73] C. F. Barenghi, R. J. Donnelly, and W. F. Vinen, J. Low. Temp. Phys. **52**, 189 (1983).
[74] See Supplemental Material at http://link.aps.org/supplemental/10.1103/PhysRevE.94.043101 for the tables listing the multiscaling exponents from the different set of runs.
[75] J. Salort, B. Chabaud, E. Lévêque, and P.-E. Roche, J. Phys.: Conf. Ser. **318**, 042014 (2011).